D_1 Optical Pumping of Rubidium Isotopes ^{87}Rb and ^{85}Rb

Bhaskar Mookerji and Charles Herder*
MIT Department of Physics
(Dated: April 20, 2008)

We experimentally characterize the weak-field Zeeman perturbation on the $5^2S_{1/2}$ state of ^{87}Rb ($I = 3/2$) and ^{85}Rb ($I = 5/2$). Optically pumping rubidium vapor with a 794nm circularly polarized light source, we determine the electronic g_F-factors to be 0.3341 ± 0.0009 (^{85}Rb) and 0.5010 ± 0.0009 (^{87}Rb). In the process of canceling the ambient magnetic field, we determine the local magnetic field to be $(375 \pm 10, 60 \pm 15, 190 \pm 10)$mG. The Bohr magneton and relative isotope abundance of ^{87}Rb and ^{85}Rb are determined to be $(9.29 \pm 0.03) \times 10^{-24}$J/T and $0.45 \pm 0.02/0.55 \pm 0.02$. Finally, we discuss the parameter dependence of relaxation rates of optical pumping on gas temperature and optical density of our source.

The method of optically pumping the magnetic Zeeman states of an alkali gas are instrumental in the construction of lasers and atomic clocks, and has furthermore formed a historical basis through which laser manipulation techniques, such as a laser cooling and ion trapping, have been applied to atomic physics.

Through the selective absorption and emission of circularly polarized light, the populations of the magnetic Zeeman states can be dramatically altered from their thermal Maxwell-Boltzmann distribution. In the following, we will first discuss the weak-field Zeeman splitting of rubidium and the optical pumping of those states. We will describe optical pumping apparatus and its rubidium vapor source, and measure the parameter characterizing the Zeeman splittings, the electronic g-factors of the rubidium isotopes. We will also discuss relaxation effects from an alternating magnetic field.

1. WEAK-FIELD ZEEMAN SPLITTING AND OPTICAL PUMPING

Our investigations into the degeneracy splitting of electronic structure in alkali atoms have largely been limited to magnetic field perturbations internal to the structure of the atom, namely fine and hyperfine structure. Our measurement of of the nuclear magnetic moment in this experiment uses a weak external magnetic field to induce Zeeman splitting among hyperfine energy states. The magnetic dipole moments associated with the total electron angular momentum $\mathbf{J} = \mathbf{L} + \mathbf{S}$ and the total angular momentum $\mathbf{F} = \mathbf{J} + \mathbf{I}$ of the atom are given by,

$$\mu_J = -g_J \cdot \frac{\mu_B}{\hbar}\mathbf{J} \qquad \mu_F = -g_I \cdot \frac{\mu_n}{\hbar}\mathbf{I}, \tag{1}$$

where g parametrizes the magnitude of the magnetic moment, μ_B is the Bohr magneton (9.24×10^{-24}J/T), and $\mathbf{L}$, $\mathbf{S}$, and $\mathbf{I}$ are the appropriate atomic spins. The energy levels of a $5^2S_{1/2}$ electronic state of an alkali atom in an external magnetic field $\mathbf{B}$ is given by,

$$H = A\mathbf{I} \cdot \mathbf{J} + g_J \mu_0 \mathbf{J} \cdot \mathbf{B} + g_I \mu_0 \mathbf{I} \cdot \mathbf{B}, \tag{2}$$

where A is the magnetic dipole constant describing the strength of the hyperfine interaction. If the energy shift due to the magnetic field is small compared to the fine and hyperfine splittings, the energy difference between Zeeman states is simply given by

$$\Delta E_{|Fm_F\rangle} = \mu_B g_F m_F B_z, \tag{3}$$

where, through a complete set of commuting observables, the electron g factors are,

$$g_F = g_J \frac{F(F+1) + J(J+1) - I(I+1)}{2F(F+1)}, \tag{4}$$

and

$$g_J = 1 + \frac{J(J+1) + S(S+1) - L(L+1)}{2L(L+1)}. \tag{5}$$

These g_F-factor evaluates to 1/3 and 1/2 for ^{85}Rb ($I = 5/2$) and ^{87}Rb ($I = 3/2$), respectively.

The goal of optical pumping is to preferentially alter the thermal distribution of populations among the Zeeman states. Photons at 780nm excite absorption transitions from the $5^2S_{1/2}$ to the $^2P_{1/2}$, and angular momentum selection rules allow transitions among Zeeman states such that $\Delta m_F = 0, \pm 1$. Circularly polarized light can convey an angular momentum $\hbar$ parallel to the magnetic field $\mathbf{B}$ and restricts this absorption selection rule to $\Delta m_F = 1$. Spontaneous emission from the final state obeys the selection rule $\Delta m_F = 0, \pm 1$, and the continual absorption and emission of photons collect all the atoms in the highest $5^2S_{1/2}$ ($F = 1$) Zeeman substate, $m_F = 1$.

1.1. Relaxation Effects

Polarized rubidium atoms in the optically-pumped $m_F = 1$ state become depolarized upon collisions with the boundaries of the vapor cell. Following Benumof [1],

*Electronic address: mookerji@mit.edu; URL: http://web.mit.edu/8.13/

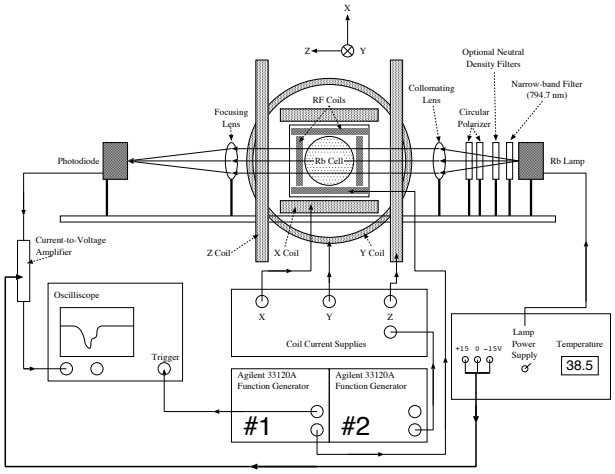

FIG. 1: Optical pumping apparatus.

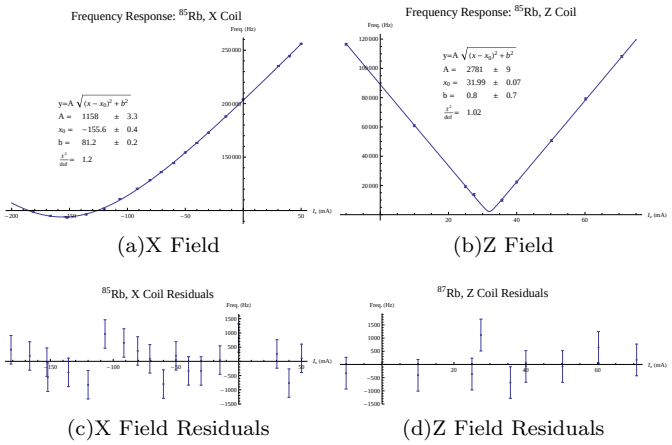

FIG. 2: Resonant frequency dependence on x and z applied Helmholtz current and residuals. Our ambient field parameter B_{z0} is determined at the local minimum of the hyperbola. Breaks in the residuals occur at points where we alter the frequency range of our sweep.

we derive the relaxation dynamics of optical pumping in a ground state which will later be applicable to our determination of relaxation times. The probabilities of transition up to the $m_F = 1$ state from any ground state and down from the $m_F = 1$ are given by $W_u dt$ and $W_d dt$, respectively. The populations n of the optically-pumped $m_F = 1$ state and N of all other ground states are described by the coupled rate equations:

$$\frac{dN}{dt} = nW_d - NW_u \qquad \frac{dn}{dt} = NW_u - nW_d. \tag{6}$$

Therefore, when a constant field is turned on, the number of atoms in the optically pumped state asymptotically approaches a maximum, while the remaining ground state populations are similarly reduced.

For a relaxation time $\tau = (W_u + W_d)^{-1}$, factor $C = \tau(N_0 W_u - n_0 W_d)$, and baseline light intensity I_0, the intensity I of transmitted light through the vapor cell is taken as a function of the excess atoms in the $m_F = 1$ state. The rate equations yield:

$$I = I_0 + \alpha(n - N) = I_0 + \alpha C\left(1 - e^{-t/\tau}\right). \tag{7}$$

2. EXPERIMENTAL SETUP AND PROCEDURE

A schematic of our experimental setup is in Figure 2. A rubidium RF discharge lamp excites valence electrons to the $5^2P_{1/2}$ (or higher) state and the spontaneously emitted photons pass through a 794.7nm narrow-band optical filter. The resulting beam is doppler broadened around the $5^2S_{1/2} \rightarrow 5^2P_{1/2}$ D_1 transition. The beam passes through a circular polarizer (a linear polarizer and a quarter-wave plate) and is focused to maximize intensity through a gas absorption cell. In addition to our rubidium gas, the absorption cell contains a non-polar buffer gas (neon) to minimize depolarizing collisions among rubidium atoms and with the boundary of the absorption cell. The absorption cell is also contained within a plexiglass oven whose temperature is coarsely determined by a 120V Variac transformer and monitored by a thermocouple at or above rubidium's boiling point (38.5°). The intensity of the transmitted light from the rubidium cell is measured by a solidstate photodiode and current amplifier connected to a dual-trace oscilloscope.

Our optical setup also allows us to apply various direct and alternating magnetic fields to the rubidium gas. With our absorption cell at the center, three Helmholtz coils (x, y, and z) are DC biased in the mA range to cancel out the ambient magnetic field. The Helmoholtz coil along the optical axis (z) can also apply alternating magnetic fields (square or sawtooth) to measure the Zeeman splitting and various relaxation effects. An RF coil in x can irradiate the vapor with RF photons, inducing transitions among Zeeman substates. The magnetic field produced by a current I through a Helmholtz coil of radius R and total turns N is given by

$$B = \frac{8\mu_0 R^2 N}{\sqrt{125}R} I = \frac{8\mu_0 R^2 N}{\sqrt{125}R} \frac{\Delta V}{Z}. \tag{8}$$

For voltage sweeps, the magnetic field is determined from the resistive impedance Z across the coils ($48.7 \pm 0.1\Omega$).

3. RESULTS AND ERROR ANALYSIS

For our determination of the local ambient magnetic field, electronic g factors, and isotope abundance, we varied the strength of the magnetic field by incrementing the current bias on the Helmholtz coils while sweeping the RF coils between 1 and 400 kHz. Fixing the field in two directions and incrementing the current bias in

one direction, we can shift the resonant frequency to a global minimum, at which point we have approximately canceled the ambient field. A plot of the resonant frequency as a function of applied current (mA) is found in Figure 3, where center frequencies are determined using oscilloscope cursors. The required quantities are determined by expressing the resonant frequency in terms of the applied field. The resonant frequency in a given direction as a function of the applied magnetic field is given by

$$\nu = \frac{g_f \mu_B}{h}|\mathbf{B}| = \frac{g_f \mu_B}{h}\sqrt{(B - B_{z0})^2 + B_{xy}}, \qquad (9)$$

where B_{z0} is the ambient field in the z direction (for example), B is the applied magnetic field in that direction, and B_{xy} is the applied field in the remaining directions.

TABLE I: Measured ambient magnetic field, Bohr magneton, and g factor for ^{85}Rb and ^{87}Rb.

	^{85}Rb (mG)	^{87}Rb (mG)	Hall Probe (mG)
B_x	385 ± 1.1	382 ± 1.0	375 ± 10
B_y	61 ± 3.0	61 ± 2.0	60 ± 15
B_z	183.7 ± 0.5	183.9 ± 0.5	190 ± 10
	μ_B (J/T)	μ_B (J/T)	
X	$(9.29 \pm 0.03) * 10^{-24}$	$(9.30 \pm 0.02 * 10^{-24}$	
Y	$(10.0 \pm 1.2) * 10^{-24}$	$(10.0 \pm 0.8) * 10^{-24}$	
Z	$(9.76 \pm 0.4) * 10^{-24}$	$(9.70 \pm 0.4) * 10^{-24}$	
	g_f	g_f	
X	0.3341 ± 0.0009	0.5010 ± 0.0009	
Y	0.360 ± 0.04	0.54 ± 0.04	
Z	0.35 ± 0.02	0.52 ± 0.02	

We measured the local ambient magnetic field twice: first, using the resonances in the rubidium gas, and second, using a Hall gaussmeter. These values values are given in Table I and are in excellent agreement with each other. According to NOAA's National Geographic Data Center (NGDC), the estimated magnetic field of the Earth at Boston is $\mathbf{B} = (491.8, 51.8, 190.0)$mG, which is in agreement with all but one of our measured values [2]. A likely explanation is the presence of other magnetic materials contributing to our ambient field.

Also determined from Equation 9 are the g factors and the Bohr magneton given in Table I, each within 1σ of accepted values for each of our measurements. Note that these values cannot be determined independently of each other, so theoretical values were assumed for one or the other when fitting for the g factors and the Bohr magneton. Furthermore, the accuracy and error of measurements in a given direction is limited in part by the range of the Helmholtz power supply. This is particularly true for the limited range of the y coil and the decreased signal-to-noise ratio for our z coil measurement.

We also determined relative abundances of the rubidium isotopes in our absorption cell. We measured peak heights using vertical oscilloscope cursors for 15 equally-spaced current biases on the x Helmholtz coil. Peak heights ranged between 3 and 13mV with an voltage error of 0.2-0.5mV from the oscilloscope's resolution. With these values, the relative isotope abundances of ^{87}Rb and ^{85}Rb are determined to be $0.45 \pm 0.02/0.55 \pm 0.02$.

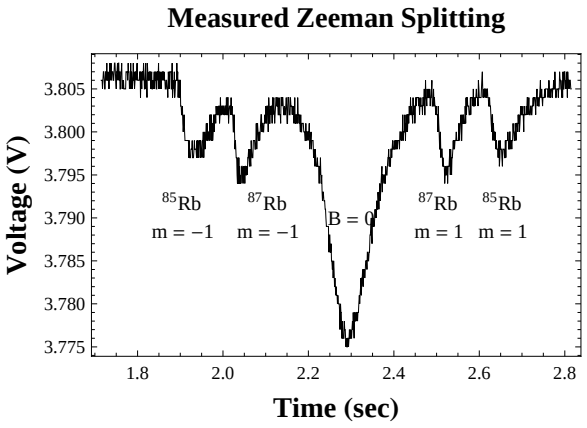

FIG. 3: Zeeman splitting of $5^2S_{1/2}(F = 1)$ for ^{85}Rb and ^{87}Rb. The center peak corresponds to the zero-field Zeeman degeneracy, whereas the inner(outer) peaks correspond to $m_F = \pm 1$ of ^{85}Rb (^{87}Rb).

Fixing the applied resonance frequency, we can map the Zeeman spectrum by applying a voltage sawtooth that sweeps the applied **B**-field of the vapor cell. The result is shown in Figure 3. Several features in the asymmetry of the Zeeman spectrum are notable. The sharp absorption results from the complete depolarization of optically-pumped atoms during the voltage sweep. The finite slope of the absorption line, like many of the following spectra that constitute depolarization, corresponds to static field inhomogeneities in our arrangement to cancel Earth's magnetic field. When the rubidium reapproaches polarization in the optically pumped state, the intensity returns to baseline. Note that the relaxation time and sweep time asymmetrically broaden the measured scope capture.

3.1. Depolarization Parameters

In the second part of this experiment, we drive the RF coils at the resonant frequency of a transition, alternate the magnetization in the optical axis, and measure the relaxation and attenuation effects of optical density and temperature parameters of our optical pumping. Note first that relaxation and attenuation are independent of the strength of the alternating field, which only alters the resonant frequency of photon absorption. A sample relaxation curve is in Figure 3.1. We fit the relaxation curve using the Lev-Marquardt fitting algorithm in Mathematica 6, and resulting offsets and relaxation times for ^{8}7Rb are included in Figure 5. The errors from the dc offset

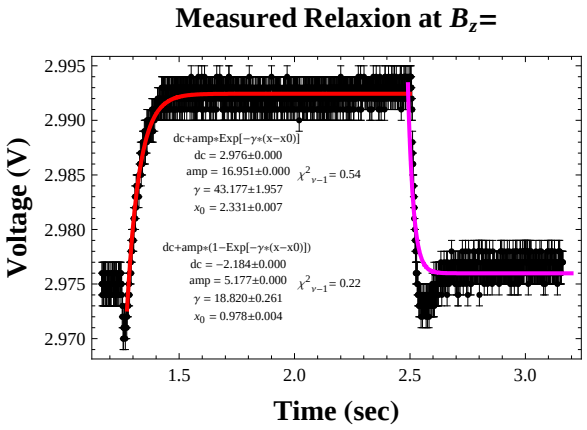

FIG. 4: Example relaxation curve from alternating field. The dip below baseline intensity corresponds to inductive kickback through the lab function generator.

and relaxation parameters are used in our later characterization of optical attenuation and temperature.

At constant temperature 44.3°C, we measure the voltage response of the vapor cell through a series of optical density filters (0.1, 0.2, 0.3, and 0.7). The DC voltage offset is logarithmically related to the optical density of the transmitted light. Relaxation times saturate toward higher values of optical density and range between 0.078 and 0.11ms with increasing attenuation. These trends are expected, as the attenuated photons entering the rubidium vapor would take longer to optically pump to the $m_F = 1$ states.

With no optical attenuation, we measure the voltage response of the vapor cell through a series of evenly spaced temperatures between 33° and 45°. Because gas pressure increases with temperature in the cell, we expect an increase in depolarizing collisions and a corresponding increase in relaxation times. The DC voltage offset is linearly related to the temperature, while relaxation rates seem more or less random. However, review papers on optical pumping have suggested particularly non-linear dependence of relaxation time and pressure of the buffer gas a rubidium cell [3].

4. ERROR ANALYSIS AND CONCLUSIONS

Using optical pumping, we have successfully measured the electronic g factors and the Bohr magneton. The accuracy and error of our magnetic field measurements make this technique preferable over using a Hall gaussmeter for magnetometry. Particularly true for the relaxation measurements, sample time and oscilloscope resolution reduced the signal-to-noise ratio in our data, introducing a significant source of error into our fits for relaxation times and DC offsets. Temperature control with the Variac, as it has been for many other temperature measurements in lab, was rough and difficult to maintain at thermal equilibrium. The measurement of ambient light by the photodiode and a baseline background noise from mechanical vibrations, in addition to our resolution introduce a systematic error on the order of a mV.

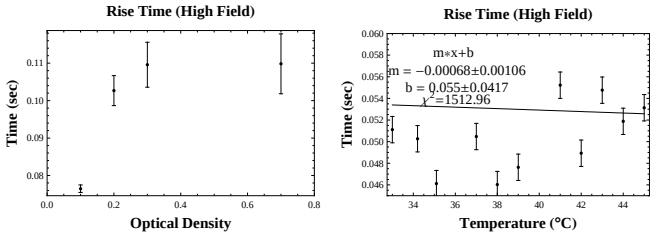

(a)Optical relaxation times (b)Temperature relaxation times

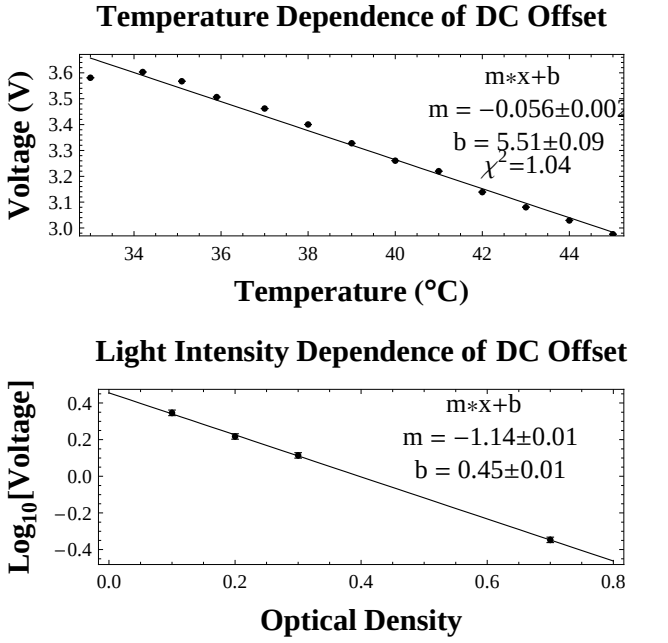

FIG. 5: Parameter dependence of relaxation times and DC offsets for ^{8}7Rb.

[1] R. Benumof, Am. J. Phys. pp. 151–160 (1963).
[2] (2008), URL http://www.ngdc.noaa.gov/geomag/magfield.shtml.
[3] P. Happer, Rev. Mod. Phys. p. 210 (1972).